Available online at www.sciencedirect.com
ScienceDirect
Comput. Methods Appl. Mech. Engrg. 278 (2014) 388–403
Computer methods in applied mechanics and engineering
www.elsevier.com/locate/cma

Discrete double directors shell element for the functionally graded material shell structures analysis

M. Wali*, A. Hajlaoui, F. Dammak

Mechanical Modelization and Manufacturing Laboratory (LA2MP), National Engineering School of Sfax, B.P W3038, Sfax, University of Sfax, Tunisia

Received 24 December 2013; received in revised form 28 March 2014; accepted 7 May 2014
Available online 11 June 2014

Abstract

In this paper, the accuracy and the efficiency of the 3d-shell model based on a double directors shell element for the functionally graded material (FGM) shell structures analysis is studied. The vanishing of transverse shear strains on top and bottom faces is considered in a discrete form. Thus, the third-order shear deformation plate theory (TSDT) is a particular case of the discrete double directors shell model (DDDSM) used in the present work. The DDDSM is introduced to remove the shear correction factors, when using the first-order shear deformation theory (FSDT), and improve an excellent performance when compared with other works. This model can be used for static, free vibration and buckling analyses of FGM. The convergence of the proposed model is compared to other well-known formulations found in the literature.

Keywords: FGM; Shell element; Third-order deformation theory

1. Introduction

In recent years, shell structures made of FGMs are widely used in many engineering fields such as aerospace, gas turbines, nuclear fusions, electronics, etc. because they present many advantages. Indeed, they are used in systems which need high heat-resistance, high rigidity and eventually absence of the interface problem unlike laminate structures. The material properties of FGMs are inhomogeneous and vary continuously in one or more directions. Typical FGMs are made from a mixture of ceramic and metal, or a combination of different metals or different ceramics that are appropriate to achieve the desired objective.

The importance of this kind of materials motivates many contemporary researchers to study their properties and behaviors. Among these studies, we mention works of Vel and Batra [1] who presented the three dimensional exact solution for free and forced vibrations of functionally graded rectangular plates, Ferreira et al. [2] who studied the static deformations of functionally graded plates using the radial basis function collocation method and a higher-order shear deformation theory, they selected the shape parameter in the radial basis functions by an optimization procedure based on the cross validation technique.

Matsunaga [3] calculated the natural frequencies and buckling stresses of plates made of FGMs using a 2-D higher-order deformation theory. Carrera et al. [4] evaluated the effect of thickness stretching in plate/shell structures made by FGM in the thickness directions. Neves et al. [5] presented a quasi-3d hyperbolic shear deformation theory for the

* Corresponding author. Tel.: +216 20385960; fax: +216 74666535.
E-mail address: mondherwali@yahoo.fr (M. Wali).

http://dx.doi.org/10.1016/j.cma.2014.05.011
0045-7825/

bending and free vibration analysis of functionally graded plates. Xiang et al. [6] used an n-order shear deformation theory and a meshless global collocation method based on the thin plate spline radial basis function to analyze the static characteristics of functionally graded plates under sinusoidal load.

The study of FGM structures using classical theory, based on the Kirchhoff hypothesis, is lack of precision. The inaccuracy is due to neglecting the effects of transverse shear and normal strains of the structure. In order to take into account the effects of gradual change of material properties, the first-order shear deformation theory (FSDT) and higher-order shear deformation theories (HSDT) have been used in the analyses of FGMs. However, since using the FSDT, shear correction factors should be incorporated to adjust the transverse shear stiffness and the accuracy of solutions will be strongly dependent on the correction factors. Examples of the FSDT approach are given in [7,8].

To analyze static and dynamic behavior of FGMs, a number of theoretical formulations and finite element models based on the HSDT were developed. Reddy [9] presented a general formulation for FGMs using the third-order shear deformation plate theory and developed the associated finite element model that accounts for the thermo-mechanical coupling and geometric non-linearity. Numerous works using HSDT are published to study the transverse shear deformations through the FGM shell thickness, such as [10–12].

On the other hand, to model the multi-layered structures capable to take into account the strong discontinuities in material properties across the thickness, a multi-directors shell theory has been used in the literature. In this approach, the theories of shells are considered as oriented 2D areas with additional kinematic variables modeling the shell behavior. Such continuous domain is known as Cosserat surface [13]. In the same context, Başar et al. [14] developed a refined finite-rotation theory with seven independent displacement variables for arbitrary multilayered shell structures made particularly of composite material layers. This theory approximates the displacement field by a cubic series expansion of thickness coordinates, which imply a quadratic shear deformation distribution across the thickness. Başar et al. [15] presented a multi-directors shell theory on the basis of a quadratic approximation of the displacement field. Their contribution is the development of four-node isoparametric shell elements providing an accurate prediction of interlaminar stresses in composite laminates; special attention is given to the consideration of finite rotations as well as large deformations. An enriched kinematic field in order to extend the potential application domain of the shell model is developed by Brank and Carrera [16], Brank et al. [17] and Brank [18]. In these works, the researchers discussed a theoretical formulation of shell model accounting for through-the-thickness stretching, which allows large deformations and direct use of 3d constitutive equations.

The primary objective of this work is to study FGM shell structures. The problem formulation is established from an adopted 3d-shell nonlinear model based on a double directors shell element. However, this paper treats only linear FGM shell structure by linearizing equations obtained from the developed non-linear DDDSM formulation with a third-order deformation theory. The linearized model is validated both by standard tests and by comparing the accuracy and the performance with works in the literature. In fact, the used double directors shell model is developed in [19] to study constant elastic materials and extended in this paper for FGM shell structures. The third-order shear deformation plate theory of Reddy [20] and Reddy [9], is the linear version of the DDDSM model projected in a 2d xy-plane. In the modeling, the vanishing of transverse shear strains on top and bottom faces is considered in a discrete form, similar to the development of the nonlinear discrete Kirchhoff shell element presented in the work of Dammak et al. [21].

The outline of the paper is as follows. In Section 2, the material properties of the functionally graded materials are illustrated. In Sections 3 and 4 the kinematic of the double directors shell model and the weak form of shell equilibrium equations are presented respectively. The implemented finite elements are described in Section 5. A number of numerical simulations are presented in Section 6 and closing remarks are stated in Section 7.

2. Material properties

An FGM shell structure with polynomial material law, as given by Zenkour [22], is considered. The shell structure is graded from aluminum (bottom surface) to alumina (top surface) materials. The following functional relationship is considered for the Young modulus $E_{\mathrm{FGM}}(z)$ in the thickness direction:

$$E_{\mathrm{FGM}}(z) = E_m + (E_c - E_m)\left(\frac{z}{h} + \frac{1}{2}\right)^n \tag{1}$$

where $E_m = 70$ GPa and $E_c = 380$ GPa are the Young modulus of the metal and ceramic components, respectively and n is the power-law index. The Poisson ratio for both metal and ceramic is assumed to be constant and equal to $\nu = 0.3$.

3. Basic concepts of the model

In this section, the geometry and kinematic of nonlinear double directors shell model are described. The fixed spatial coordinate system is defined by a triad $(\mathbf{E}_i)$, $i = 1, 2, 3$. The reference surface of the shell is assumed to be smooth, continuous and differentiable. Initial and current configurations of the shell, are denoted, respectively, by C_0 and C_t. Variables associated with the undeformed state C_0 will be denoted by upper-case letters and by lower-case letters when referred to the deformed configuration C_t. Vectors will be denoted by bold letters.

3.1. Double directors shell kinematic hypothesis

Parameterizations of the shell material points are carried out in terms of curvilinear coordinates $\boldsymbol{\xi} = (\xi^1, \xi^2, \xi^3 = z)$. The position vectors of any material point (q), whose normal projection on mid-surface is the material point (p), in the initial states C_0 are given by

$$\boldsymbol{X}_q\left(\xi^1, \xi^2, z\right) = \boldsymbol{X}_p\left(\xi^1, \xi^2\right) + z\,\boldsymbol{D}\left(\xi^1, \xi^2\right), \quad z \in [-h/2, h/2] \tag{2}$$

where h is the thickness, p is a point of the reference surface, and $\boldsymbol{D}$ is the initial shell director. The base vectors, in the initial state C_0 are given as

$$\boldsymbol{G}_\alpha = \boldsymbol{A}_\alpha + z\,\boldsymbol{D}_{,\alpha}; \qquad \boldsymbol{G}_3 = \boldsymbol{D}, \quad \alpha = 1, 2. \tag{3}$$

The surface element dA in the initial state is given by

$$dA = \sqrt{A}\,dA_\xi, \quad \sqrt{A} = \|\boldsymbol{A}_1 \wedge \boldsymbol{A}_2\|, \; dA_\xi = d\xi^1 d\xi^2. \tag{4}$$

The covariant reference metric tensor $\boldsymbol{G}$ at a material point $\boldsymbol{\xi}$ is defined by

$$\boldsymbol{G} = \left[\boldsymbol{G}_i \cdot \boldsymbol{G}_j\right], \quad i, j = 1, 2, 3. \tag{5}$$

For later use geometrical variables are added

$$\textit{Determinant } G\text{: } \sqrt{G} = [\boldsymbol{G}_1\,\boldsymbol{G}_2\,\boldsymbol{G}_3] = \sqrt{|G_{ij}|} \tag{6}$$

$$\textit{Volume element}\text{: } dV = \sqrt{G}\,d\xi^1 d\xi^2 dz. \tag{7}$$

With the hypothesis of a double directors shell model, the position vector of the point q in the deformed configuration is given by:

$$\boldsymbol{x}_q\left(\xi^1, \xi^2, z\right) = \boldsymbol{x}_p\left(\xi^1, \xi^2\right) + f_1(z)\,\boldsymbol{d}_1\left(\xi^1, \xi^2\right) + f_2(z)\,\boldsymbol{d}_2\left(\xi^1, \xi^2\right). \tag{8}$$

The base vectors, in the deformed state are then

$$\boldsymbol{g}_\alpha = \boldsymbol{a}_\alpha + f_1(z)\,\boldsymbol{d}_{1,\alpha} + f_2(z)\,\boldsymbol{d}_{2,\alpha}; \qquad \boldsymbol{g}_3 = f_1'(z)\,\boldsymbol{d}_1 + f_2'(z)\,\boldsymbol{d}_2. \tag{9}$$

The metric tensor components in C_t are separated into the in-plane and out-of-plane part components. With some approximations, the metric tensor can be written as

$$g_{ij} = \boldsymbol{g}_i \cdot \boldsymbol{g}_j, \qquad \begin{cases} g_{\alpha\beta} \approx a_{\alpha\beta} + f_1(z)\,b^1_{\alpha\beta} + f_2(z)\,b^2_{\alpha\beta} \\ g_{\alpha 3} \approx f_1'(z)\,c^1_\alpha + f_2'(z)\,c^2_\alpha \qquad\qquad \alpha, \beta = 1, 2 \\ g_{33} \approx \left(f_1' + f_2'\right)^2 d, \end{cases} \tag{10}$$

where $a_{\alpha\beta}$, $b^k_{\alpha\beta}$ and c^k_α $(k = 1, 2)$ represent the covariant metric surface, the first curvature tensors and the shear, respectively. The parameter d presents the thickness stretching.

Taking into account $\boldsymbol{d}_1 \cdot \boldsymbol{d}_1 \approx \boldsymbol{d}_2 \cdot \boldsymbol{d}_2 \approx \boldsymbol{d}_1 \cdot \boldsymbol{d}_2$, these components can be computed as

$$\begin{cases} a_{\alpha\beta} = \boldsymbol{a}_\alpha \cdot \boldsymbol{a}_\beta, \qquad c^k_\alpha = \boldsymbol{a}_\alpha \cdot \boldsymbol{d}_k \\ b^k_{\alpha\beta} = \boldsymbol{a}_\alpha \cdot \boldsymbol{d}_{k,\beta} + \boldsymbol{a}_\beta \cdot \boldsymbol{d}_{k,\alpha}, \qquad d = \boldsymbol{d}_1 \cdot \boldsymbol{d}_1, \end{cases} \quad k = 1, 2. \tag{11}$$

Similar expressions for the in-plane and out-of-plane components of the metric tensor can be obtained in the case of the initial configuration C_0.

3.2. Strain measure

Using Eq. (10), the Lagrangian strain $\boldsymbol{E}$ has the following components:

$$\boldsymbol{E} = \frac{1}{2}\left(\boldsymbol{g} - \boldsymbol{G}\right), \qquad E_{ij} = \frac{1}{2}\left(g_{ij} - G_{ij}\right), \qquad \begin{cases} E_{\alpha\beta} = e_{\alpha\beta} + f_1(z)\,\chi^1_{\alpha\beta} + f_2(z)\,\chi^2_{\alpha\beta} \\ 2E_{\alpha 3} = f_1'(z)\,\gamma^1_\alpha + f_2'(z)\,\gamma^2_\alpha \\ E_{33} = 1/2\left[\left(f_1' + f_2'\right)^2 d - 1\right] \end{cases} \tag{12}$$

where $e_{\alpha\beta}$ denote the membrane strains, $\chi^k_{\alpha\beta}$ the bending strains and γ^k_α the shear strains, which can be computed as

$$\begin{cases} e_{\alpha\beta} = \left(a_{\alpha\beta} - A_{\alpha\beta}\right)/2, \qquad \gamma^k_\alpha = c^k_\alpha - C^k_\alpha \\ \chi^k_{\alpha\beta} = \left(b^k_{\alpha\beta} - B^k_{\alpha\beta}\right)/2, \end{cases} \qquad k = 1, 2. \tag{13}$$

In matrix notation, the vectors of membrane, bending and shear strains are given by:

$$\boldsymbol{e} = \begin{Bmatrix} e_{11} \\ e_{22} \\ 2e_{12} \end{Bmatrix}, \qquad \boldsymbol{\chi}^k = \begin{Bmatrix} \chi^k_{11} \\ \chi^k_{22} \\ 2\,\chi^k_{12} \end{Bmatrix}, \qquad \boldsymbol{\gamma}^k = \begin{Bmatrix} \gamma^k_1 \\ \gamma^k_2 \end{Bmatrix}, \quad k = 1, 2. \tag{14}$$

To impose a third-order double directors shell model and at the same time a quadratic distribution of the shear stress, the following expressions for $f_1(z)$ and $f_2(z)$ are chosen

$$f_1(z) = z - f_2(z), \qquad f_2(z) = 4z^3/3h^2. \tag{15}$$

This gives the following shear strain

$$2E_{\alpha 3} = f_1'(z)\,\gamma^1_\alpha + f_2'(z)\,\gamma^2_\alpha = \left(1 - 4\frac{z^2}{h^2}\right)\gamma^1_\alpha + 4\frac{z^2}{h^2}\gamma^2_\alpha. \tag{16}$$

Vanishing of the transverse shear stress on the top and bottom shell faces, $\sigma_{yz}(\pm h/2) = \sigma_{xz}(\pm h/2) = 0$, the shear strain can be obtained as follows:

$$\gamma^2_\alpha = 0, \qquad 2E_{\alpha 3} = \left(1 - 4z^2/h^2\right)\gamma^1_\alpha. \tag{17}$$

This kinematic constraint will be imposed in a discrete form in the finite element approximation.

4. Weak form and linearization

By using the total Lagrangian formulation, the weak form of equilibrium equations is given as

$$G = \int_V S^{ij}\,\delta E_{ij}\,dV - G_{ext} = 0 \tag{18}$$

where dV is the shell volume element in the initial configuration, δE_{ij} are the covariant components of the virtual Green–Lagrange strain tensor, S^{ij} are the contravariant components of the second Piola–Kirchhoff stress tensor and G_{ext} is the external virtual work. Performing the integration through the thickness of the shell, and using Eqs. (12) and (17), the weak form becomes

$$G = \int_A \left(\boldsymbol{N}\cdot\delta\boldsymbol{e} + \sum_{k=1}^{2}\boldsymbol{M}_k\cdot\delta\boldsymbol{\chi}^k + \boldsymbol{T}_1\cdot\delta\boldsymbol{\gamma}^1\right)dA - G_{ext} = 0 \tag{19}$$

where $\delta \boldsymbol{e}$, $\delta \boldsymbol{\chi}^k$ and $\delta \boldsymbol{\gamma}^1$ are the variations of shell strains and $\boldsymbol{N}, \boldsymbol{M}_k$ and $\boldsymbol{T}_1$ are the membrane, bending and shear stresses resultants which can be written as

$$\boldsymbol{N} = \begin{Bmatrix} N^{11} \\ N^{22} \\ N^{12} \end{Bmatrix}, \qquad \boldsymbol{M}_k = \begin{Bmatrix} M_k^{11} \\ M_k^{22} \\ M_k^{12} \end{Bmatrix}, \qquad \boldsymbol{T}_1 = \begin{Bmatrix} T_1^1 \\ T_1^2 \end{Bmatrix} \quad k = 1, 2. \tag{20}$$

These components are defined as follows

$$N^{\alpha\beta} = \int_{-h/2}^{h/2} S^{\alpha\beta} \sqrt{G/A}\, dz, \qquad M_k^{\alpha\beta} = \int_{-h/2}^{h/2} f_k(z)\, S^{\alpha\beta} \sqrt{G/A} dz$$
$$T_1^{\alpha} = \int_{-h/2}^{h/2} f_1'(z)\, S^{\alpha 3} \sqrt{G/A}\, dz. \tag{21}$$

The virtual strains can be obtained as the variation of the strain measures which yields from Eq. (13)

$$\begin{cases} \delta \mathrm{e}_{\alpha\beta} = 1/2 \left(\boldsymbol{a}_\alpha \cdot \delta \boldsymbol{x}_{,\beta} + \boldsymbol{a}_\beta \cdot \delta \boldsymbol{x}_{,\alpha} \right), \qquad \delta \gamma_\alpha^1 = \boldsymbol{a}_\alpha \cdot \delta \boldsymbol{d}_1 + \delta \boldsymbol{x}_{,\alpha} \cdot \boldsymbol{d}_1 \\ \delta \chi_{\alpha\beta}^k = 1/2 \left(\boldsymbol{a}_\alpha \cdot \delta \boldsymbol{d}_{\mathrm{k},\beta} + \boldsymbol{a}_\beta \cdot \delta \boldsymbol{d}_{\mathrm{k},\alpha} + \delta \boldsymbol{x}_{,\alpha} \cdot \boldsymbol{d}_{\mathrm{k},\beta} + \delta \boldsymbol{x}_{,\beta} \cdot \boldsymbol{d}_{\mathrm{k},\alpha} \right). \end{cases} \tag{22}$$

Moreover, by defining the generalized resultant vectors of stress and strain with

$$\boldsymbol{R} = \begin{Bmatrix} \boldsymbol{N} \\ \boldsymbol{M}_1 \\ \boldsymbol{M}_2 \\ \boldsymbol{T}_1 \end{Bmatrix}_{11\times 1}, \qquad \boldsymbol{\Sigma} = \begin{Bmatrix} \boldsymbol{e} \\ \boldsymbol{\chi}^1 \\ \boldsymbol{\chi}^2 \\ \boldsymbol{\gamma}^1 \end{Bmatrix}_{11\times 1} \tag{23}$$

the weak form of the equilibrium equation can be rewritten as

$$G(\boldsymbol{\Phi}, \delta\boldsymbol{\Phi}) = \int_A \delta \boldsymbol{\Sigma}^T \cdot \boldsymbol{R} dA - G_{ext}(\boldsymbol{\Phi},\ \delta\boldsymbol{\Phi}) = 0 \tag{24}$$

where $\boldsymbol{\Phi} = (\boldsymbol{u}, \boldsymbol{d}_1, \boldsymbol{d}_2)$. Eq. (24) defines the nonlinear shell problem, which can be solved by the Newton iterative procedure. The consistent tangent operator for the Newton solution procedure can be constructed by the directional derivative of the weak form in the direction of the increment $\Delta\boldsymbol{\Phi} = (\Delta\boldsymbol{u}, \Delta\boldsymbol{d}_1, \Delta\boldsymbol{d}_2)$. It is a conventional practice to split the tangent operator into geometric and material parts, denoted by $D_G G \cdot \boldsymbol{\Delta\Phi}$ and $D_M G \cdot \boldsymbol{\Delta\Phi}$, respectively, i.e,

$$DG \cdot \boldsymbol{\Delta\Phi} = D_G G \cdot \boldsymbol{\Delta\Phi} + D_M G \cdot \boldsymbol{\Delta\Phi}. \tag{25}$$

The geometric part results from the variation of the virtual strains while holding stress resultants constant:

$$D_G G \cdot \boldsymbol{\Delta\Phi} = \int_A \left(\boldsymbol{\Delta\delta\Sigma}^T \cdot \boldsymbol{R} \right) dA. \tag{26}$$

This geometric part is not developed in this paper. The material part of the tangent operator results from the variation in the stress resultants and thus takes the form

$$D_M G \cdot \boldsymbol{\Delta\Phi} = \int_A \delta \boldsymbol{\Sigma}^T \cdot \boldsymbol{\Delta R} dA = \int_A \delta \boldsymbol{\Sigma}^T \cdot \boldsymbol{H}_T \cdot \Delta\boldsymbol{\Sigma} dA \tag{27}$$

where $\boldsymbol{H}_T$ is the material tangent modulus, expressed as

$$\boldsymbol{H}_T = \begin{bmatrix} \boldsymbol{H}_{11} & \boldsymbol{H}_{12} & \boldsymbol{H}_{13} & 0 \\ & \boldsymbol{H}_{22} & \boldsymbol{H}_{23} & 0 \\ & & \boldsymbol{H}_{33} & 0 \\ Sym & & & \boldsymbol{H}_{44} \end{bmatrix} \tag{28}$$

$$(\boldsymbol{H}_{11}, \boldsymbol{H}_{12}, \boldsymbol{H}_{13}, \boldsymbol{H}_{22}, \boldsymbol{H}_{23}, \boldsymbol{H}_{33}) = \int_{-h/2}^{h/2} \left(1, f_1, f_2, f_1^2, f_1 f_2, f_2^2\right) \boldsymbol{H} dz \tag{29}$$

$$\boldsymbol{H}_{44} = \int_{-h/2}^{h/2} \left(f_1'\right)^2 \boldsymbol{H}_\tau dz \tag{30}$$

where $\boldsymbol{H}$ and $\boldsymbol{H}_\tau$ are in plane and out-of-plane linear elastic sub-matrices, which can be expressed in the Cartesian system as

$$\boldsymbol{H} = \frac{E(z)}{1-\nu^2(z)} \begin{bmatrix} 1 & \nu(z) & 0 \\ \nu(z) & 1 & 0 \\ 0 & 0 & (1-\nu(z))/2 \end{bmatrix}, \qquad \boldsymbol{H}_\tau = \frac{E(z)}{2(1+\nu(z))} \begin{bmatrix} 1 & 0 \\ 0 & 1 \end{bmatrix}. \tag{31}$$

5. Remarks on finite element approximation

In this section, the numerical implementation of the presented shell theoretical formulation based upon a four node non-linear shell element is established. The displacement vector is defined as: $\boldsymbol{u} = \boldsymbol{x}_p - \boldsymbol{X}_p$. Using the isoparametric concept, the variation and incremental of displacement vector is approximated by

$$\delta\boldsymbol{u} = \sum_{I=1}^{4} N^I \delta\boldsymbol{u}_I, \qquad \Delta\boldsymbol{u} = \sum_{I=1}^{4} N^I \Delta\boldsymbol{u}_I \tag{32}$$

where N^I are the standard isoparametric shape functions. The isoparametric concept is illustrated in detail in the work of [23]. The first director vector $\boldsymbol{d}_1$ is approximated with the same functions

$$\delta\boldsymbol{d}_1 = \sum_{I=1}^{4} N^I \delta\boldsymbol{d}_{1I}, \qquad \Delta\boldsymbol{d}_1 = \sum_{I=1}^{4} N^I \Delta\boldsymbol{d}_{1I}. \tag{33}$$

5.1. Membrane and first bending strain field

The shell membrane part of the problem is considered. The strain–displacement relation is

$$\delta\boldsymbol{e} = \boldsymbol{B}_m \cdot \delta\boldsymbol{\Phi}_n \tag{34}$$

where $\boldsymbol{\Phi}_n$ is the nodal variables and $\boldsymbol{B}_m$ is the discrete membrane strain–displacement operator defined as

$$\boldsymbol{B}_m^I = \begin{bmatrix} \boldsymbol{B}_{mm}^I & \boldsymbol{0} & \boldsymbol{0} \end{bmatrix}, \qquad \boldsymbol{B}_{mm}^I = \begin{bmatrix} \boldsymbol{a}_1^T N_{,1}^I \\ \boldsymbol{a}_2^T N_{,2}^I \\ \boldsymbol{a}_1^T N_{,2}^I + \boldsymbol{a}_2^T N_{,1}^I \end{bmatrix}. \tag{35}$$

For the first bending part, the strain–displacement relation is given by

$$\delta\boldsymbol{\chi}^1 = \boldsymbol{B}_1 \cdot \delta\boldsymbol{\Phi}_n, \tag{36}$$

where $\boldsymbol{B}_1$ is the discrete first bending strain–displacement operator

$$\boldsymbol{B}_1^I = \begin{bmatrix} \boldsymbol{B}_{1m}^I & \boldsymbol{B}_{1b}^I & \boldsymbol{0} \end{bmatrix}, \qquad \boldsymbol{B}_{1m}^I = \begin{bmatrix} \boldsymbol{d}_{1,1}^T N_{,1}^I \\ \boldsymbol{d}_{1,2}^T N_{,2}^I \\ \boldsymbol{d}_{1,1}^T N_{,2}^I + \boldsymbol{d}_{1,2}^T N_{,1}^I \end{bmatrix}, \qquad \boldsymbol{B}_{1b}^I = \begin{bmatrix} \boldsymbol{a}_1^T N_{,1}^I \\ \boldsymbol{a}_2^T N_{,2}^I \\ \boldsymbol{a}_1^T N_{,2}^I + \boldsymbol{a}_2^T N_{,1}^I \end{bmatrix}. \tag{37}$$

5.2. Construction of the assumed natural transverse shear strain field

A typical isoparametric shell element is considered as depicted in Fig. 1. A, B, C and D denote the mid-points of the element boundaries set. The assumed natural transverse shear strain field is expressed by Bathe and Dvorkin [24]

$$\delta\boldsymbol{\gamma}^1 = \begin{bmatrix} \delta\gamma_1^1 \\ \delta\gamma_2^1 \end{bmatrix} = \begin{bmatrix} (1-\eta)\,\delta\gamma_1^1(B) + (1-\eta)\,\delta\gamma_1^1(D) \\ (1-\xi)\,\delta\gamma_2^1(A) + (1-\xi)\,\delta\gamma_2^1(C) \end{bmatrix} \tag{38}$$

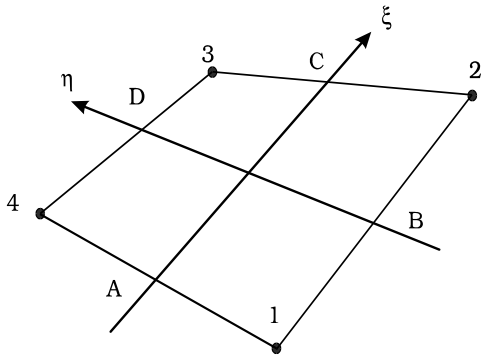

Fig. 1. Assumed strain construction of the isoparametric shell element.

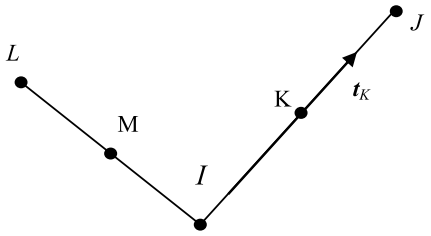

Fig. 2. Position of the nodes couple (I, J).

where $\gamma_2^1(A)$, $\gamma_1^1(B)$, $\gamma_2^1(C)$ et $\gamma_1^1(D)$ are the transverse shear strains at points as defined in Fig. 1.

$$\delta\boldsymbol{\gamma}^1 = \boldsymbol{B}_s \cdot \delta\boldsymbol{\Phi}_n \tag{39}$$

where $\boldsymbol{B}_s$ is the discrete shear strain–displacement operator

$$\boldsymbol{B}_s = \begin{bmatrix} N^1_{,1}\boldsymbol{d}^T_{1B} & N^2_{,1}\boldsymbol{a}^T_{1B} & \boldsymbol{0} & N^2_{,1}\boldsymbol{d}^T_{1B} & N^2_{,1}\boldsymbol{a}^T_{1B} & \boldsymbol{0} & N^3_{,1}\boldsymbol{d}^T_{1D} & N^3_{,1}\boldsymbol{a}^T_{1D} & \boldsymbol{0} & N^4_{,1}\boldsymbol{d}^T_{1D} & N^3_{,1}\boldsymbol{a}^T_{1D} & \boldsymbol{0} \\ N^1_{,2}\boldsymbol{d}^T_{1A} & N^4_{,2}\boldsymbol{a}^T_{2A} & \boldsymbol{0} & N^2_{,2}\boldsymbol{d}^T_{1C} & N^3_{,2}\boldsymbol{a}^T_{2C} & \boldsymbol{0} & N^3_{,2}\boldsymbol{d}^T_{1C} & N^3_{,2}\boldsymbol{a}^T_{2C} & \boldsymbol{0} & N^4_{,2}\boldsymbol{d}^T_{1A} & N^4_{,2}\boldsymbol{a}^T_{2A} & \boldsymbol{0} \end{bmatrix}. \tag{40}$$

5.3. Discrete constraints

The shear part relative to the second director vector $\boldsymbol{d}_2$ is vanished in a discrete form. A quadratic interpolation is used as proposed in the work of [21].

$$\delta\boldsymbol{d}_2 = \sum_{I=1}^{4} N^I \delta\boldsymbol{d}_{2I} + \sum_{K=5}^{8} P_K \delta\alpha_K \boldsymbol{t}_K, \qquad \Delta\boldsymbol{d}_2 = \sum_{I=1}^{4} N^I \Delta\boldsymbol{d}_{2I} + \sum_{K=5}^{8} P_K \Delta\alpha_K \boldsymbol{t}_K \tag{41}$$

where (I) represents a node of the element, (K) represents the mid-point of the element boundaries and $\delta\alpha_K$ are variables associated to $\delta\boldsymbol{d}_2$ on the element boundaries. The vector $\boldsymbol{t}_K$ is unit and its direction is defined by the position of the nodes couple (I, J) as shown in Fig. 2.

$$\boldsymbol{t}_K = (\boldsymbol{x}_J - \boldsymbol{x}_I)/L_K, \quad L_K = \|\boldsymbol{x}_J - \boldsymbol{x}_I\| \tag{42}$$

where L_K is the $I - J$ side length. The shape functions P_K are quadratic and are given in Table 1.

By introducing the vanishing shearing hypothesis, on top and bottom faces, over the element boundaries under integral form, the transverse strain is given for side (I, J) by

$$\int_I^J \delta\gamma^2_{sz} ds = 0, \tag{43}$$

$$\delta\gamma^2_{sz} = \delta\beta_s + \delta\boldsymbol{u}_{,s} \cdot \boldsymbol{d}_2, \qquad \delta\beta_s = \boldsymbol{t}_K \cdot \delta\boldsymbol{d}_2 \tag{44}$$

Table 1
Functions P_K.

P_K	$P_5 = 0.5\left(1-\xi^2\right)(1-\eta)$
	$P_6 = 0.5\,(1+\xi)\left(1-\eta^2\right)$
	$P_7 = 0.5\left(1-\xi^2\right)(1+\eta)$
	$P_8 = 0.5\,(1-\xi\,)\left(1-\eta^2\right)$

where (s) is a parametric coordinate. While using a linear interpolation of the displacement vector $\delta\boldsymbol{u}$, this vector can be written for the side (I, J) as follows:

$$\delta\boldsymbol{u} = (1-\xi)\,\delta\boldsymbol{u}_I + \xi\delta\boldsymbol{u}_J, \quad 0 \le \xi = s/L_K \le 1. \tag{45}$$

The director vector $\boldsymbol{d}_2$ is given by

$$\boldsymbol{d}_2 = \frac{\tilde{\boldsymbol{d}}}{\left\|\tilde{\boldsymbol{d}}\right\|}, \qquad \tilde{\boldsymbol{d}} = \sum_{I=1}^{4} N^I \boldsymbol{d}_{2I} \tag{46}$$

$$\delta\boldsymbol{d}_2 = \frac{1}{\left\|\tilde{\boldsymbol{d}}\right\|}\boldsymbol{P}_d\,\delta\tilde{\boldsymbol{d}}, \qquad \boldsymbol{P}_d = \boldsymbol{I} - \boldsymbol{d}_2 \otimes \boldsymbol{d}_2 \tag{47}$$

where $\boldsymbol{P}_d$ is an orthogonal projection. Vector $\delta\tilde{\boldsymbol{d}}$ is defined by a quadratic interpolation as in Eq. (37):

$$\delta\tilde{\boldsymbol{d}} = (1-\xi)\,\delta\boldsymbol{d}_I + \xi\delta\boldsymbol{d}_J + 4\xi\,(1-\xi)\,\delta\alpha_K\boldsymbol{t}_K. \tag{48}$$

Then the final expression of $\delta\beta_s$ is

$$\delta\beta_s \approx \frac{1}{\left\|\tilde{\boldsymbol{d}}\right\|}\left((1-\xi)\,\delta\beta_{sI} + \xi\delta\beta_{sJ} + 4\xi\,(1-\xi)\,\delta\alpha_K\right). \tag{49}$$

Then to integrate the two terms of the vanishing shearing hypothesis, the relations (44), (45) and (49) are used

$$\int_I^J \delta\boldsymbol{u}_{,s}\cdot\boldsymbol{d}_2\,ds \approx (\delta\boldsymbol{u}_I + \delta\boldsymbol{u}_J)\,\frac{(\boldsymbol{d}_I + \boldsymbol{d}_J)}{\|\boldsymbol{d}_I + \boldsymbol{d}_J\|} \tag{50}$$

$$\int_I^J \delta\beta_s\,ds \approx \frac{L_K}{\|\boldsymbol{d}_I + \boldsymbol{d}_J\|}\left(\delta\beta_{sI} + \delta\beta_{sJ} + \frac{4}{3}\delta\alpha_K\right). \tag{51}$$

The constraint is obtained by taking the sum of these last two equations equal to zero. This leads to the following expression of variables $\delta\alpha_k$

$$\delta\alpha_K = \frac{3}{2L_K}\left((\delta\boldsymbol{u}_I + \delta\boldsymbol{u}_J)\cdot\boldsymbol{d}_K - \frac{3}{4}(\delta\boldsymbol{d}_I + \delta\boldsymbol{d}_J)\cdot\boldsymbol{t}_K\right) \tag{52}$$

$$\boldsymbol{d}_K = \frac{1}{2}(\boldsymbol{d}_I + \boldsymbol{d}_J). \tag{53}$$

The expression of the director vector $\boldsymbol{d}_2$ is deduced from interpolation (41)

$$\delta\boldsymbol{d}_2 = \sum_{I=1}^{4} N^I\delta\boldsymbol{d}_{2I} + \sum_{K=5}^{8}\frac{3}{2}P_K\,(1/L_K\,(\delta\boldsymbol{u}_I + \delta\boldsymbol{u}_J)\cdot\boldsymbol{d}_K - 1/2\,(\delta\boldsymbol{d}_I + \delta\boldsymbol{d}_J)\cdot\boldsymbol{t}_K)\,\boldsymbol{t}_K. \tag{54}$$

In a matrix form, the director vector $\boldsymbol{d}_2$ is written as

$$\delta\boldsymbol{d}_2 = \sum_{I=1}^{4}\left(\boldsymbol{M}_d^I\delta\boldsymbol{u}_I + \boldsymbol{M}_r^I\delta\boldsymbol{d}_{2I}\right) \tag{55}$$

where matrices $\boldsymbol{M}_d^I$ and $\boldsymbol{M}_r^I$ are given by

$$\boldsymbol{M}_d^I = P_K \boldsymbol{td}_K^I + P_M \boldsymbol{td}_M^I, \quad \boldsymbol{td}_K^I = \frac{3}{2L_K} \boldsymbol{t}_K \otimes \boldsymbol{d}_K \tag{56}$$

$$\boldsymbol{M}_r^I = N^I \boldsymbol{I} + P_K \boldsymbol{tt}_K^I + P_M \boldsymbol{tt}_M^I, \quad \boldsymbol{tt}_K^I = \frac{3}{4} \boldsymbol{t}_K \otimes \boldsymbol{t}_K. \tag{57}$$

The (K) and (M) are the two mid-sides of each side of the quadrilateral, which are bound to the node (I) (Fig. 2). Finally, the second bending strain is expressed as

$$\delta \boldsymbol{\chi}^2 = \boldsymbol{B}_2 \cdot \delta \boldsymbol{\Phi}_n \tag{58}$$

where $\boldsymbol{B}_2$ is the discrete second bending strain–displacement operator

$$\boldsymbol{B}_2^I = \begin{bmatrix} \boldsymbol{B}_{2m}^I & \boldsymbol{0} & \boldsymbol{B}_{2b}^I \end{bmatrix} \tag{59}$$

$$\boldsymbol{B}_{2m}^I = \begin{bmatrix} \boldsymbol{d}_{2,1}^t N_{,1}^I + \boldsymbol{a}_1^t \cdot \boldsymbol{M}_{d,1}^I \\ \boldsymbol{d}_{2,2}^t N_{,2}^I + \boldsymbol{a}_2^t \cdot \boldsymbol{M}_{d,2}^I \\ \boldsymbol{d}_{2,1}^t N_{,2}^I + \boldsymbol{d}_{2,2}^t N_{,1}^I + \boldsymbol{a}_1^t \cdot \boldsymbol{M}_{d,2}^I + \boldsymbol{a}_2^t \cdot \boldsymbol{M}_{d,1}^I \end{bmatrix}, \qquad \boldsymbol{B}_{2b}^I = \begin{bmatrix} \boldsymbol{a}_1^t \cdot \boldsymbol{M}_{r,1}^I \\ \boldsymbol{a}_2^t \cdot \boldsymbol{M}_{r,2}^I \\ \boldsymbol{a}_1^t \cdot \boldsymbol{M}_{r,2}^I + \boldsymbol{a}_2^t \cdot \boldsymbol{M}_{r,1}^I \end{bmatrix}. \tag{60}$$

Finally, the generalized strain $\delta \boldsymbol{\Sigma}$ can be expressed as follows

$$\delta \boldsymbol{\Sigma} = \begin{Bmatrix} \delta \boldsymbol{e} \\ \delta \boldsymbol{\chi}^1 \\ \delta \boldsymbol{\chi}^2 \\ \delta \boldsymbol{\gamma}^1 \end{Bmatrix} = \boldsymbol{B} \cdot \delta \boldsymbol{\Phi}_n, \qquad \boldsymbol{B} = \begin{bmatrix} \boldsymbol{B}_m \\ \boldsymbol{B}_1 \\ \boldsymbol{B}_2 \\ \boldsymbol{B}_s \end{bmatrix}. \tag{61}$$

5.4. Nodal transformation

In all equations, $\delta \boldsymbol{d}_k$ and $\delta \boldsymbol{d}_{k,\alpha}$ are the variation of the directors and their derivatives. These variations can be written either in spatial description as

$$\delta \boldsymbol{d}_k = \delta \boldsymbol{\theta}_k \wedge \boldsymbol{d}_k = \boldsymbol{\Lambda}_k \, \delta \boldsymbol{\theta}_k, \qquad \bar{\boldsymbol{\Lambda}}_k = -\tilde{\boldsymbol{d}}_k \tag{62}$$

where $\tilde{\boldsymbol{d}}_k$ is the skew-symmetric tensor such that $\tilde{\boldsymbol{d}}_k \boldsymbol{d}_k = \boldsymbol{0}$, or in material description

$$\delta \boldsymbol{d}_k = \boldsymbol{Q}_k \, \delta \bar{\boldsymbol{\Theta}}_k \, \boldsymbol{E}_3 = \bar{\boldsymbol{\Lambda}}_k \delta \boldsymbol{\Theta}_k, \quad \bar{\boldsymbol{\Lambda}}_k = \boldsymbol{Q}_k \tilde{\boldsymbol{E}}_3 \tag{63}$$

where $\boldsymbol{d}_k = \boldsymbol{Q}_k \boldsymbol{E}_3$ and $\boldsymbol{E}_3 = \begin{bmatrix} 0 & 0 & 1 \end{bmatrix}^t$.

A spatial description leads to a shell problem with 9 DOF/node and the material description leads to a shell problem with 7 DOF/node. The transformation $\bar{\boldsymbol{\Lambda}}$ in the material description takes the following form

$$\bar{\boldsymbol{\Lambda}}_k = \begin{bmatrix} -\boldsymbol{t}_{2k} & \boldsymbol{t}_{1k} \end{bmatrix}_{3\times 2}. \tag{64}$$

6. Numerical examples

The performance of the proposed discrete double directors shell element is evaluated with several problems. The convergence of the results is compared to other well-known formulations. A listing of these shell elements, and their abbreviations is presented in Table 2.

The results given with the S4 element are obtained with the addition of an automatic calculation of the shear correction factors as in [25]. A P-FGM that consists of the following properties: (E_c, E_m, ν, n) is considered. All material and geometrical properties are given in a coherent system of units.

6.1. Bending of a rhombic plate

A simply supported rhombic plate of side $L = 100$ mm, thickness $h = 1$ mm and power-law index $n = 6$ is uniformly pressure loaded: $q = 1$ MPa. The center-point deflection is normalized with the finite element converged

Table 2
Listing of shell elements.

Name	Description
SQAD4	Discrete Kirchhoff quadrilateral of [21]
S4	First order shear deformable shell element of [7]
SHO4	Present double directors shell element

Table 3
Center-point deflection of a rhombic plate.

Node per side	SQAD4	S4	Present	
			SHO4	%
3	13.76	1.842	7.846	240.08
5	5.670	2.760	5.186	158.69
9	3.873	2.821	3.695	113.06
17	3.417	3.028	3.348	102.44
33	3.286	3.166	3.279	100.33

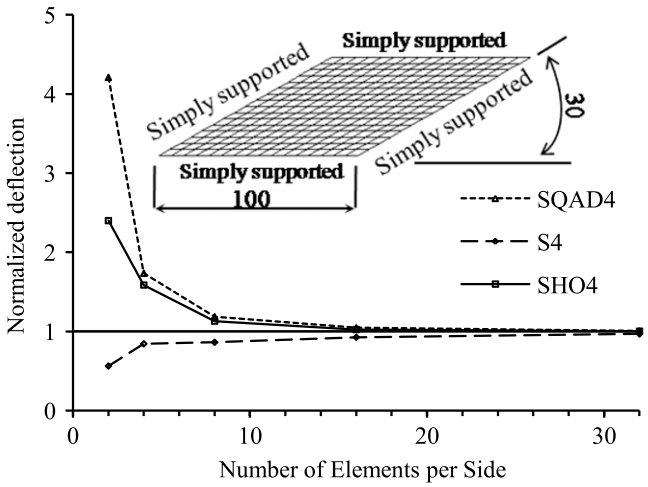

Fig. 3. Description and results of the rhombic plate under uniform pressure loading.

solution of 3.268 using 100 elements per side. The difficulty in this problem arises from the singularity of the solution at the obtuse vertices, where the stresses tend to infinity [7]. To assess the convergence of shell elements, the uniform mesh shown in Fig. 3 is used. The results are listed in Table 3 and shown in Fig. 3.

6.2. Pinched hemispherical shell with 18° hole

A pinched hemispherical shell with an 18° hole at the top, shown in Fig. 4, with two inward and two outward forces 90° apart is modeled using symmetry boundary conditions on one quadrant. This problem is a good test of the inextensional bending behavior of an element, and an excellent test for the ability of an element to model rigid-body motions [7]. Material and geometric properties for this test are $n = 6$, radius $R = 10$ m, and thickness $h = 0.04$ m. The numerical results are presented in Table 4 and Fig. 4, normalized with the finite element converged solution of 5.232×10^{-2} using 100 elements per side.

6.3. Pinched cylinder with end diaphragms

A short cylinder, with two pinching vertical forces at the middle section, and two rigid diaphragms at the end, is modeled using one octant and applying the appropriate symmetry boundary conditions (Fig. 5). The length of the cylinder is $L = 600$ mm, the radius is $R = 30$ mm, and the thickness is $h = 3$ mm. The power-law index $n = 6$.

Table 4
Hemispherical shell with 18° hole ($\times 10^{-2}$).

Node per side	SQAD4	S4	Present	
			SHO4	%
3	5.266	4.709	5.185	99.10
5	5.440	5.216	5.398	103.17
9	5.286	5.188	5.269	100.70
17	5.223	5.198	5.220	99.77
33	5.225	5.223	5.229	99.94

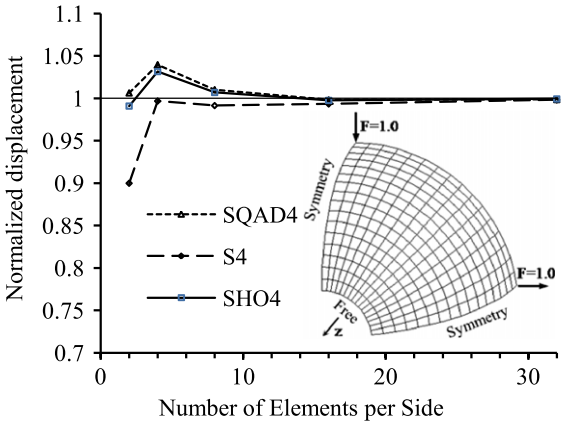

Fig. 4. Description and results of the pinched hemisphere with an 18° hole. Symmetry is used and only one quadrant is modeled.

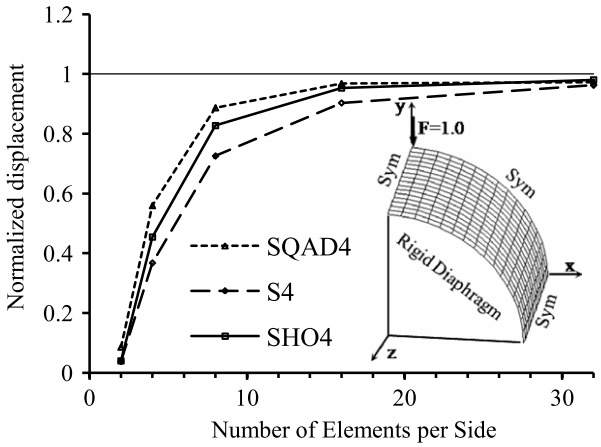

Fig. 5. Description and results of the pinched cylinder with end diaphragms. Symmetry is used and only one eighth of the cylinder is modeled.

The numerical results are presented in Table 5 and Fig. 5, normalized with the finite element converged solution of 4.7468×10^{-4} using 100 elements per side. This problem is the most demanding of all considered cases. It is a severe test of the inextensional bending and complex membrane states of stress. Most four node shell elements do not converge efficiently in this problem.

It can be found from Fig. 3 to 5 that the present model, SHO4, produces the close results to those of SQAD4 and S4 elements. Also, for these three tests, it is noticed that the proposed model exhibits high performance even with coarse mesh.

Table 5
Pinched cylinder with end diaphragms ($\times 10^{-4}$).

Node per side	SQAD4	S4	Present	
			SHO4	%
3	0.408	0.181	0.189	3.98
5	2.657	1.745	2.157	45.44
9	4.211	3.445	3.928	82.75
17	4.594	4.288	4.525	95.32
33	4.618	4.569	4.654	98.04

Table 6
Dimensionless parameters of FGM square plate ($a/h = 10$) under sinusoidal load.

n	Method	$\bar{w}$	$\bar{\sigma}_x$	$\bar{\sigma}_y$	$\bar{\tau}_{xy}$	$\bar{\tau}_{xz}$	$\bar{\tau}_{yz}$
1	Zenkour [22]	0.5889	3.0870	1.4894	0.6110	0.2462	0.2622
	Present SHO4	0.5886	3.0970	1.4910	0.6093	0.2381	0.2602
	Carrera et al. [26]	0.5875	–	–	–	–	–
	Xiang et al. [6]	0.5895	3.2480	1.5287	0.6295	–	–
2	Zenkour [22]	0.7573	3.6094	1.3954	0.5441	0.2265	0.2763
	Present SHO4	0.7568	3.6200	1.3980	0.5426	0.2181	0.2731
	Carrera et al. [26]	0.7570	–	–	–	–	–
	Xiang et al. [6]	0.7581	3.7062	1.4222	0.5559	–	–
4	Zenkour [22]	0.8819	4.0693	1.1783	0.5667	0.2029	0.2580
	Present SHO4	0.8810	4.0800	1.1810	0.5652	0.1940	0.2532
	Carrera et al. [26]	0.8823	–	–	–	–	–
	Xiang et al. [6]	0.8824	3.9371	1.1474	0.5620	–	–
7	Zenkour [22]	0.9562	4.5971	0.9903	0.5834	0.2081	0.2194
	Present SHO4	0.9552	4.6090	0.9925	0.5818	0.1989	0.2152
	Carrera et al. [26]	0.9554	–	–	–	–	–
	Xiang et al. [6]	0.9563	4.6568	1.0026	0.5868	–	–

6.4. Square plate under static doubly sinusoidal load

This test consists of square FGM plate under static doubly sinusoidal distributed load q expressed as $q = q_0 \sin(\pi x/a) \sin(\pi y/a)$ (Fig. 6). A 20×20 meshing is used for this validation test. The used dimensionless parameters are

$$\bar{w} = \frac{10E_c h^3}{a^4 q_0} w\left(\frac{a}{2}, \frac{a}{2}\right), \qquad \bar{\sigma}_x = \frac{h}{aq_0}\sigma_x\left(\frac{a}{2}, \frac{a}{2}, \frac{h}{2}\right), \qquad \bar{\sigma}_y = \frac{h}{aq_0}\sigma_y\left(\frac{a}{2}, \frac{a}{2}, \frac{h}{3}\right)$$
$$\overline{\sigma}_{xy} = \frac{h}{aq_0}\sigma_{xy}\left(0, 0, -\frac{h}{3}\right), \qquad \overline{\sigma}_{yz} = \frac{h}{aq_0}\sigma_{yz}\left(\frac{a}{2}, 0, \frac{h}{6}\right), \qquad \overline{\sigma}_{xz} = \frac{h}{aq_0}\sigma_{xz}\left(0, \frac{a}{2}, 0\right).$$

Table 6 lists the dimensionless displacements and stresses of a simply supported FGM square plate of ($a/h = 10$). It can be found that the results obtained by the present model are in good agreement with those found in the works of [22,26,6]. In addition, the obtained results are nearly close to those of [22].

The distribution across the plate thickness of the dimensionless shear stress $\overline{\sigma}_{xz} = \frac{h}{aq_0}\sigma_{xz}\left(0, \frac{a}{2}, 0\right)$ for various values of the exponent n, using 20×20 meshes, is illustrated in Fig. 7 and is compared with the results of the 3d solution presented in the work of [5]. The proposed DDDSM presents very close results to Neves's 3d solution. But, it is noticed from Fig. 7 that the condition of zero-transverse shear strains on top and bottom faces of the FGM plate is not considered in the work of [5].

In the following results a pined square FGM plate ($\boldsymbol{u} = \boldsymbol{0}$) submitted to static sinusoidal load is considered. A 16×16 meshing is used for these examples.

Fig. 8 shows the variation of the dimensionless center-point deflection of a square plate ($a/h = 10$) with power-law index n.

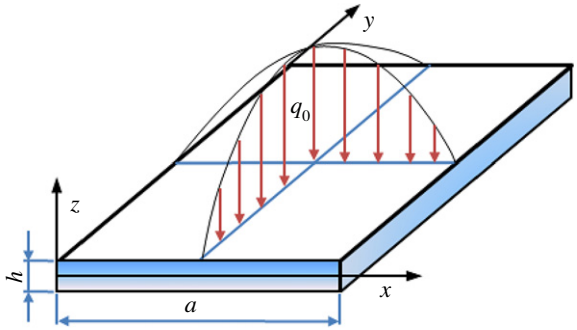

Fig. 6. A simply supported square FGM plate under sinusoidal load.

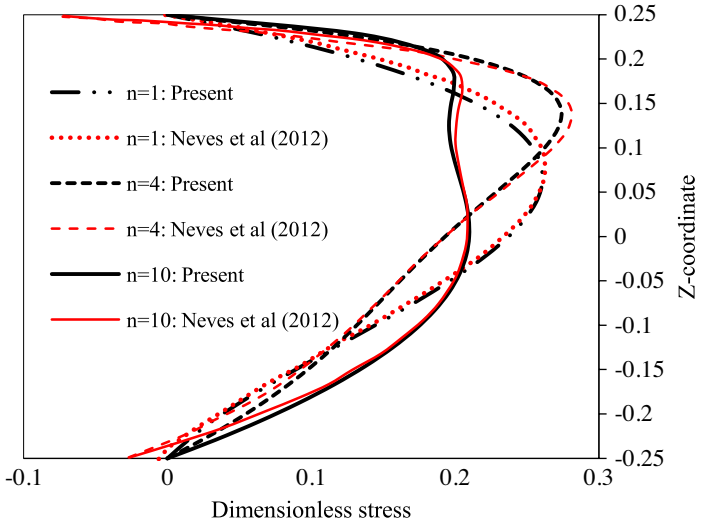

Fig. 7. Dimensionless shear stress $\bar{\sigma}_{xz}$ for a simply supported square plate under sinusoidal load ($a/h = 4$).

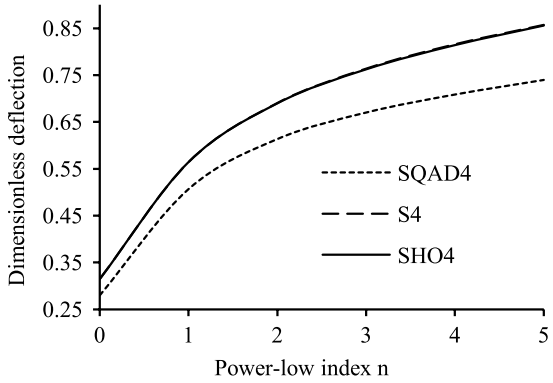

Fig. 8. Dimensionless deflection versus power law index n for a simply supported square plate under sinusoidal load ($a/h = 10$).

In Fig. 9, the dimensionless center-point deflection $\bar{w}$ is given in terms of the side-to-thickness ratio a/h for ($n = 6$). From Figs. 8 and 9 it can be easily observed that the numerical results obtained by S4 and SHO4 elements agree highly with a large variation of the ratio a/h and the power-law index n. Fig. 9 illustrates a significant discrepancy between the results obtained by the present model and Dammak et al. [21] model, especially for thick plates. This is due to the applicability ranges of the models named restriction domains. In fact, if an error of about 5%

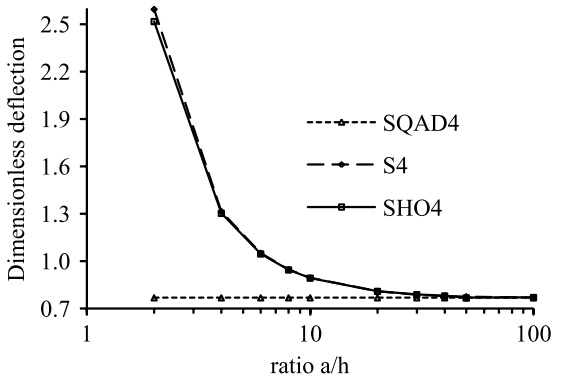

Fig. 9. Dimensionless deflection versus ratio a/h for a simply supported square plate under sinusoidal load ($n = 6$).

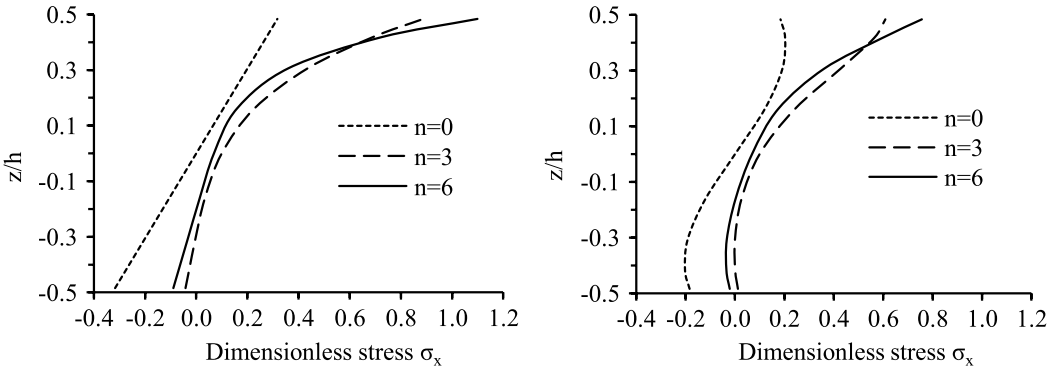

(a) First order shell theory : S4. (b) Present double directors : SHO4.

Fig. 10. Dimensionless normal stress $\bar{\sigma}_x$ for a simply supported square plate under sinusoidal load ($a/h = 10$).

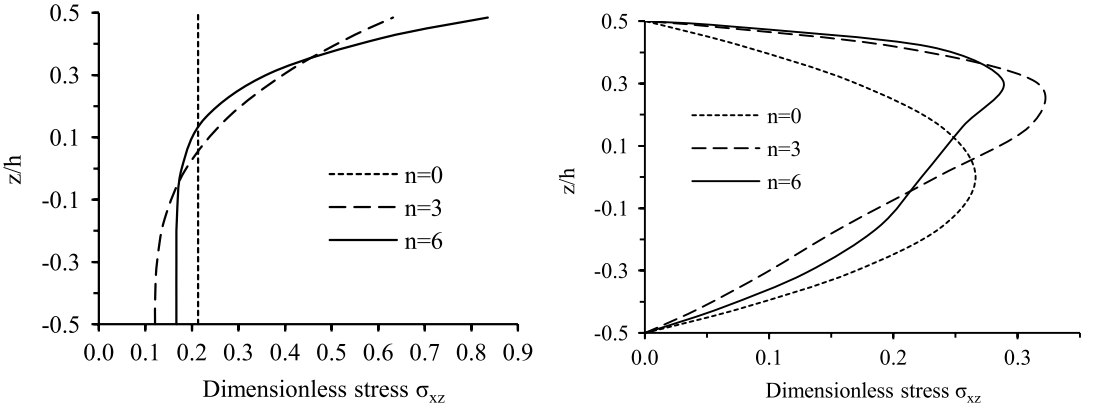

(a) First order shell theory : S4. (b) Present double directors : SHO4.

Fig. 11. Dimensionless stress $\bar{\sigma}_{xz}$ for a simply supported square plate under sinusoidal load ($a/h = 10$).

is allowed, the Mindlin–Reissner type theory can be employed for ($a/h \geq 25$) and the Kirchhoff–Love type theory only for ($a/h \geq 50$) [14].

Figs. 10 and 11 illustrate the dimensionless normal stresses $\bar{\sigma}_x = \sigma_x\,(a/2, 0)\,h^2/\left(q_0 a^2\right)$ and the dimensionless shear stresses $\bar{\sigma}_{xz} = \sigma_{xz}\,(0, a/2)\,h^2/\left(q_0 a^2\right)$, respectively versus dimensionless transverse coordinate $\bar{z} = z/h$ for different values of the power-law index n ($a/h = 10$).

From Fig. 11, it is noticed that the S4 element cannot predict accurately the dimensionless transverse stresses with the comparison of the SHO4 element.

7. Conclusions

The analysis and the efficiency of the 3d-shell model based on a double directors shell element for the FGM shell structures is presented in this paper. The transverse shear deformations are taken into account in the DDDSM model. The vanishing of transverse shear strains on top and bottom faces is considered in a discrete form. Dimensionless stresses and displacements of the simply supported functionally graded plate under sinusoidal load are computed by the present DDDSM model. By numerical investigation, the proposed model presents a good performance and high accuracy to predict the static behavior of shell structures when comparing with available published results.

The proposed (DDDSM) formulation presented in this paper can be used in the following aspects:

(a) *Linearized formulation.* This case is treated in this paper.
(b) *Free vibration.* A dynamic equation of the DDDSM model for FGM shells will be derived through Hamilton's principle.
(c) *Buckling.* Buckling stresses of shells made of FGMs will be analyzed by taking into account the effects of transverse shear deformations.
(d) *Fully nonlinear formulation.* The formulation will be assessed through numerical simulations involving the finite rotation and the geometric non-linearity.

The authors will study these aspects in future articles.

Appendix A. Supplementary data

Supplementary material related to this article can be found online at http://dx.doi.org/10.1016/j.cma.2014.05.011.

References

[1] S.S. Vel, R.C. Batra, Three-dimensional exact solution for the vibration of functionally graded rectangular plates, J. Sound Vib. 272 (2004) 703–730.
[2] A.J.M. Ferreira, C.M.C. Roque, R.M.N. Jorge, G.E. Fasshaueret, R.C. Batra, Analysis of functionally graded plates by a robust meshless method, Mech. Adv. Mater. Struct. 14 (8) (2007) 577–587.
[3] H. Matsunaga, Free vibration and stability of functionally graded plates according to a 2-D higher-order deformation theory, Compos. Struct. 82 (2008) 499–512.
[4] E. Carrera, S. Brischetto, M. Cinefra, M. Soave, Effects of thickness stretching in functionally graded plates and shells, Composites B 42 (2011) 123–133.
[5] A.M.A. Neves, A.J.M. Ferreira, E. Carrera, M. Cinefra, C.M.C. Roque, R.M.N. Jorge, C.M.M. Soares, A quasi-3D hyperbolic shear deformation theory for the static and free vibration analysis of functionally graded plates, Compos. Struct. 94 (2012) 1814–1825.
[6] S. Xiang, G.W. Kang, A nth-order shear deformation theory for the bending analysis on the functionally graded plates, Eur. J. Mech. A Solids 37 (2013) 336–343.
[7] J.C. Simo, D.D. Fox, M.S. Rifai, On a stress resultant geometrically exact shell model. Part II: The linear theory; computational aspects, Comput. Methods Appl. Mech. Engrg. 73 (1989) 53–92.
[8] J. Woo, S.A. Meguid, Nonlinear analysis of functionally graded plates and shallow shells, Int. J. Solids Struct. 38 (2001) 7409–7421.
[9] J.N. Reddy, Analysis of functionally graded plates, Internat. J. Numer. Methods Engrg. 47 (2000) 663–684.
[10] J.L. Mantari, A.S. Oktem, C.G. Soares, Static and dynamic analysis of laminated composite and sandwich plates and shells by using a new higher-order shear deformation theory, Compos. Struct. 94 (2011) 37–49.
[11] H.T. Chien, V.T. Loc, T.T. Dung, T. Nguyen-Thoi, H. Nguyen-Xuan, Analysis of laminated composite plates using higher-order shear deformation plate theory and node-based smoothed discrete shear gap method, Appl. Math. Model. 36 (2012) 5657–5677.
[12] J.L. Mantari, C.G. Soares, Optimized sinusoidal higher order shear deformation theory for the analysis of functionally graded plates and shells, Composites B 56 (2014) 126–136.
[13] C. Sansour, H. Bednarczyk, The Cosserat surface as a shell model, theory and finite-element formulation, Comput. Methods Appl. Mech. Engrg. 120 (1995) 1–32.
[14] Y. Başar, Y. Ding, R. Schltz, Refined shear-deformation models for composite laminates with finite rotations, Int. J. Solids Struct. 30 (1993) 2611–2638.
[15] Y. Başar, M. Itskov, A. Eckstein, Composite laminates: nonlinear interlaminar stress analysis by multi-layer shell elements, Comput. Methods Appl. Mech. Engrg. 185 (2000) 367–397.
[16] B. Brank, E. Carrera, A family of shear-deformable shell finite elements for composite structures, Comput. Struct. 76 (2000) 287–297.

[17] B. Brank, J. Korelc, A. Ibrahimbegovic, Nonlinear shell problem formulation accounting for through-the-thickness stretching and its finite element implementation, Comput. Struct. 80 (2002) 699–717.
[18] B. Brank, Non linear shell models with seven kinematic parameters, Comput. Methods Appl. Mech. Engrg. 194 (2005) 2336–2362.
[19] F. Dammak, Formulation isoparamétrique généralisée en analyse linéaire et non linéaire des coques par éléments finis, Ph.D. Dissertation, Laval University, Québec, Canada, 1996.
[20] J.N. Reddy, On refined computational models of composite laminates, Internat. J. Numer. Methods Engrg. 27 (1989) 361–382.
[21] F. Dammak, S. Abid, A. Gakwaya, G. Dhatt, A formulation of the non linear discrete Kirchhoff quadrilateral shell element with finite rotations and enhanced strains, Eur. J. Comput. Mech. 14 (2005) 1–26.
[22] A.M. Zenkour, Generalized shear deformation theory for bending analysis of functionally graded plates, Appl. Math. Model. 30 (2006) 67–84.
[23] G. Dhatt, G. Touzot, Une présentation de la méthode des éléments finis, Maloine S.A. Editeur, Paris et Les Presses de l'Université Laval Québec, 1981.
[24] K.J. Bathe, E. Dvorkin, A four-node plate bending element based on Mindlin/Reissner plate theory and a mixed interpolation, Internat. J. Numer. Methods Engrg. 21 (1985) 367–383.
[25] T.T. Nguyen, K. Sab, G. Bonnet, First-order shear deformation plate models for functionally graded materials, Compos. Struct. 83 (2008) 25–36.
[26] E. Carrera, S. Brischetto, A. Robaldo, Variable kinematic model for the analysis of functionally graded material plates, AIAA J. 46 (2008) 194–203.